Analyst

Cite this: *Analyst*, 2012, **137**, 2706

www.rsc.org/analyst

PAPER

Construction of an electrochemical sensor based on the electrodeposition of Au–Pt nanoparticles mixtures on multi-walled carbon nanotubes film for voltammetric determination of cefotaxime†

Saeed Shahrokhian*[ab] and Shokoufeh Rastgar[a]

Received 8th February 2012, Accepted 26th March 2012
DOI: 10.1039/c2an35182j

Mixtures of gold–platinum nanoparticles (Au–PtNPs) are fabricated consecutively on a multi-walled carbon nanotubes (MWNT) coated glassy carbon electrode (GCE) by the electrodeposition method. The surface morphology and nature of the hybrid film (Au–PtNPs/MWCNT) deposited on glassy carbon electrodes is characterized by scanning electron microscopy (SEM), energy dispersive X-ray spectroscopy (EDS), X-ray diffraction (XRD), electrochemical impedance spectroscopy (EIS) and cyclic voltammetry (CV) techniques. The modified electrode is used as a new and sensitive electrochemical sensor for the voltammetric determination of cefotaxime (CFX). The electrochemical behavior of CFX is investigated on the surface of the modified electrode using linear sweep voltammetry (LSV). The results of voltammetric studies exhibited a considerable improvement in the oxidation peak current of CFX compared to glassy carbon electrodes individually coated with MWCNT or Au–PtNPs. Under the optimized conditions, the modified electrode showed a wide linear dynamic range of 0.004–10.0 μM with a detection limit of 1.0 nM for the voltammetric determination of CFX. The modified electrode was successfully applied for the accurate determination of trace amounts of CFX in pharmaceutical and clinical preparations.

1 Introduction

In recent years, metal nanoparticles have drawn great interest in electrochemical studies because of their roles and favorable features in the fields of catalysis and sensor technology.[1–5] Bimetallic nanoparticles, in particular, show many favorable properties for researchers in comparison with the corresponding monometallic counterparts, which include high catalytic activity, catalytic selectivity, and better resistance to the deactivation difficulties. These bimetallic nanostructures have received much attention because of the modification characteristics observed not only due to the effects of nanoparticles size, but also as a result of the combination of different metals.[6–11] Carbon nanotubes (CNTs) as a catalyst-support material have drawn greater interest over the other carbon based supporting materials because of their large accessible surface areas, high stability, and high electron conductivity.[12–14] In principle, MWNTs are seamless cylinders, but they often have defect sites, where the attachment of metallic nanoparticles most likely occurs.[15] Several reports have demonstrated that uniform adsorption of metallic (or bimetallic) nanoparticles on CNT surfaces can offer new opportunities for the development of new sensors with high analytical performances.[16–18] It is well-known that the morphology and response characteristics of metal NPs greatly depend on their size, distribution and composition of nanoparticles. Therefore, it is important to develop effective methods for the preparation of nanoparticles with well-controlled composition, shape and size. Several methods have been proposed for the deposition of metal (or bi-metal) NPs on carbon nanotubes.[19–23] Electrochemical techniques are particularly attractive for the electrodeposition of metallic nanostructures on the surface of the electrode not for mass preparation in the bulk solution. In this method, various experimental parameters including solution composition, potential and time of deposition can be manipulated to control the nucleation and growth rate of the metal NPs.[24–26] Finally, electrochemical deposition is a clean, rapid and facile synthesis that facilitates control over the size and distribution of NPs, we can then use these nanoparticles with different morphologies and features in sensor applications. Among the various bimetallic nanoparticles based carbon nanotubes, Au–PtNPs have more potential applications in the area of the electrocatalysts,[27–30] electrochemical sensors[31–34] and biosensors.[35–38] Due to these advantages of bimetallic nanoparticles, it becomes significant to develop Au–Pt nanoparticles for application in electrochemical sensors with appropriate

[a]*Department of Chemistry, Sharif University of Technology, Tehran 11155-9516, Iran. E-mail: shahrokhian@sharif.edu; Fax: +98-21-66002983; Tel: +98-21-66005718*
[b]*Institute for Nanoscience and Technology, Sharif University of Technology, Tehran, Iran*
† Electronic supplementary information (ESI) available. See DOI: 10.1039/c2an35182j

characteristics such as high sensitivity, fast response time, wide linear range, better repeatability and reproducibility.

Cefotaxime (CFX) with a trade name of Claforan® (Scheme 1) is a third-generation cephalosporin antibiotic and is used to treat infections caused by bacteria, mostly respiratory and urinary infections. Like other third-generation cephalosporins, it has broad spectrum activity against Gram positive and Gram negative bacteria. The biological activity of these antibiotics is the β-lactam ring.[39,40] The major routes of CFX degradation involve hydrolysis of the β-lactam ring and the acetoxy ester. At physiologically relevant pH (pH 6–7), temperature and concentration values the amide side chain hydrolysis is negligible.[41] De-esterification proceeds more rapidly than the β-lactam ring opening. At low pHs, an internal ring closure can occur to form the lactone of the de-esterified product.[42] CFX acts by interfering with the ability of bacteria to form cell walls. The cell walls of bacteria are vital for their survival. This antibiotic impairs the bonds that hold the bacterial cell wall together. This allows holes to appear in the cell walls and kills the bacteria. CFX can also be given before certain types of surgery that are associated with an increased risk of infection, for example, abdominal, bowel, heart or bone surgery, to help prevent infections after the operation. Because of its important role in numerous pathological processes, the detection and quantification of CFX is an important feature in pharmaceutical and clinical procedures. Several methods have been reported for the determination of CFX, including spectrophotometry[43–47] and chromatography.[48–52] Though these methods give good sensitivity and selectivity they have disadvantages, including high costs, long analysis times, and the requirement of complex and tedious sample pretreatments. On the other hand, electrochemical methods have attracted great interest because of their simplicity, rapidness and high sensitivity in detecting CFX without requiring tedious pretreatments. CFX is an electroactive compound that can be oxidized and reduced electrochemically. The presence of the methoxyimino group in the cefotaxime molecule is very important for its chemical and electrochemical behavior. There are a few references in the literature dealing with CFX estimation based on cathodic reduction[53–55] and also anodic oxidation.[56–60] To the best of our knowledge, nanoparticulate hybrid materials made from metallic (bimetallic) NPs and MWCNTs have not been reported previously for the determination of this drug.

In the present work, a nanostructured thin film (as a modifier) is prepared on the surface of a glassy carbon electrode (GCE) by coating it with a thin layer of multi-walled carbon nanotubes (MWCNTs) and then the consecutive electrodeposition of AuNPs and PtNPs on the MWCNTs layer, which is capable to forming a uniform and stable thin film on the surface of the GCE. Scanning electron microscopy (SEM), energy dispersive X-ray spectroscopy (EDS), X-ray diffraction (XRD), electrochemical impedance spectroscopy (EIS) and cyclic voltammetry (CV) were used to characterize the surface of the modified electrode. The resulting electrochemical sensor under the optimum conditions is convenient and applicable for the determination of CFX with a nanomolar detection limit. Excellent features, like a low detection limit, wide linear dynamic range and high sensitivity of the modified electrode proved the successful application of this sensor for the voltammetric determination of CFX in pharmaceutical preparations and human blood serum samples.

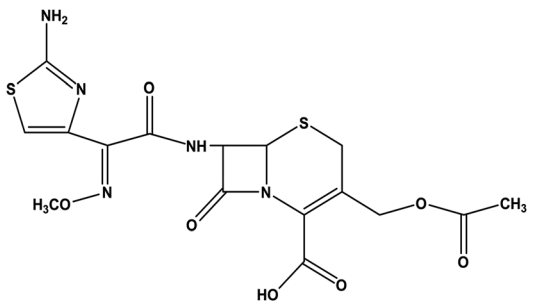

Scheme 1 Chemical structure of cefotaxime (CFX).

2 Experimental

2.1 Chemicals and reagents

Multi-walled carbon nanotubes (MWCNTs), synthesized by catalytic chemical vapor deposition (CVD) method (purity more than 95%) with o.d. (outer diameter) of 10–20 nm, i.d. (inner diameter) of 5–10 nm and tube length of 5–20 μm, was obtained from Nanostructured & Amorphous Materials (Houston, TX, USA). CFX was taken kindly from Excir Daru pharmaceutical company (Tehran–Iran). All aqueous solutions were prepared with doubly distilled deionized water. Stock solutions of CFX were freshly prepared as required in appropriate buffer solution. In all electrochemical experiments, a stock Britton–Robinson (BR) buffer solution (containing 0.04 M of glacial acetic acid, orthophosphoric acid and boric acid) was used as the supporting electrolyte. Buffer solutions of different pHs were then prepared by the addition of 0.2 M sodium hydroxide. CFX ampoules (500 mg per ampoules) were purchased from local Pharmacies. Fresh frozen human blood serum was obtained from Iranian Blood Transfusion Organization. A 2% (v/v) of pure methanol was added to the serum sample. After vortexing each of the samples for 2 min, the precipitated proteins were separated by centrifugation for 10 min at 10 000 rpm. Then, this sample was diluted 10-fold and spiked with the different amounts of standard CFX without extraction for further treatments and applied for the recovery tests in the spiked samples. Each sample was run in triplicate and relative standard deviation (RSD) for each sample was calculated. All experiments on human serum samples were performed in compliance with the relevant laws and institutional guidelines of the Sharif University of Technology.

2.2 Apparatus

Electrodeposition of Au–PtNPs on MWCNTs and voltammetric experiments were performed using a Metrohm potentiostat/galvanostat model 797VA. A conventional three-electrode system was used with a GC working electrode (unmodified or modified), a saturated Ag/AgCl reference electrode and a Pt wire counter electrode. A digital pH/mV/ion meter (CyberScan model 2500) was used for preparation of the buffer solutions. The morphologies of MWCNTs and Au–PtNPs electrodeposited on MWCNTs were obtained using with scanning electron microscope (SEM), and the composition of the Au–PtMWCNT/GC electrode was investigated by energy dispersive X-ray spectroscopy (EDS)

(RONTEC, QUANTAX). Scanning electron microscopy (SEM) images were obtained with a VEGA\\TESCAN scanning electron microscopy. The X-ray diffraction (XRD) data were collected with a MPD Model (GNR, Italian company) 3000× diffractometer that was using monochromated Cu Kα radiation (40 kV, 100 mA) and was operated using a step scan program (step width = 0.05°). All measurements were conducted at room temperature. Electrochemical impedance spectroscopy (EIS) measurements were performed with a Potentiostat/Galvanostat EG&G model 273A (Princeton Applied Research, USA) equipped with a Frequency Response Detector model 1025 (Power Suite software), which was used with a frequency between 100 MHz and 10 kHz and a 5 mV rms sinusoidal modulation (effective value of a varying AC amplitude) in 0.1 M KCl solution containing 1 mM of both $K_4Fe(CN)_6$ and $K_3Fe(CN)_6$ (1 : 1 mixture) at the $E_{1/2}$ of the $[Fe(CN)_6]^{3-/4-}$ (0.13 V *vs.* Ag/AgCl). Voltammetric experiments were carried out in buffered solutions of CFX that were deoxygenated by purging with pure nitrogen (99.999% from Roham Gas Company). Nitrogen gas was also flowed over the surface of the test solutions during the experiments.

2.3 Preparation of Au–Pt nanoparticle-modified electrodes

An appropriate amount of pure MWCNTs was treated with a 1 : 3 (v/v) mixture of HNO_3 (65%) and H_2SO_4 (98%) under reflux conditions for 6 h in order to obtain more edge sites and better dispersion of nanotubes by the creation of carboxylate groups. Before the modification, the GCE was polished with 0.1 μm alumina slurry on a polishing cloth, rinsed thoroughly with water, sonicated in water for 5 min and finally dried in air. A 3.0 mg portion of the functionalized MWCNT was dispersed in 3.0 mL DMF and homogenized ultrasonically for 10 min. Then, 3 μL of the suspension was placed on the GCE surface by micropipette and the water allowed to evaporate at 55 °C in an oven to obtain the MWCNT/GCE. The gold nanoparticles were deposited electrochemically at the MWCNT/GCE. Briefly, the MWCNT/GCE electrode was immersed into a deoxygenated solution of 0.1 mM chloroauric acid ($HAuCl_4$) in 0.5 M H_2SO_4 and a constant potential of −0.2 V (*vs.* Ag/AgCl) was applied to it for 5 s. So, AuNPs/MWCNT/GCE was prepared. In the next step, the AuNPs/MWCNT/GCE electrode was immersed in 0.5 M H_2SO_4 aqueous solution containing 1 mM hexachloroplatinic acid (H_2PtCl_6). The electrochemical deposition of the Au–PtNPs was conducted for 5 s at −0.3 V (*vs.* Ag/AgCl). Finally, Au–PtNPs/MWCNT/GCE was prepared at these optimum conditions. The Au–PtNPs/GCE was also prepared as above without the casting of the MWCNT layer on the GCE surface. Before the voltammetric measurements, the modified electrode was cycled five times between 0 and 1 V (scan rate 0.1 V s^{-1}) in a BR buffer solution of pH 2 to obtain a reproducible response. When it was necessary, renewal of the electrode surface was easily accomplished by soaking the modified electrode in BR buffer solutions and cycling the potential as mentioned above. The modified electrode was prepared daily.

3 Results and discussion

3.1 Morphological analysis

The surface morphology of the Au–PtNPs/MWCNT/GCE was characterized by SEM. As shown in Fig. 1A, a MWCNT layer without aggregation was observed on the electrode surface, indicating that the MWCNTs were homogeneously dispersed on the surface of the GCE. The diameters of the MWCNTs were approximately 25–55 nm. As can be seen in Fig. 1B, the Au–PtNPs deposited with a good distribution on the MWCNTs were spherical with an average diameter of approximately 35 nm (16–60 nm). The elemental compositions for the Au–PtNPs/MWCNTs and MWCNT samples were evaluated by EDS analysis (Fig. 2A and B). The EDS results show that, Pt and Au were the major elements on the electrode surface. The gold coatings with the same diameter (5 nm) are used during SEM analysis of MWCNT and Au–PtNPs/MWCNT modified GCE. The difference in Au content of MWCNT and Au–PtNPs/MWCNT in EDS analysis is related to the AuNPs that were electrodeposited on the surface of the MWCNT/GCE. So, the EDS results clearly show that both Au and Pt are electrodeposited in the MWCNT matrix.

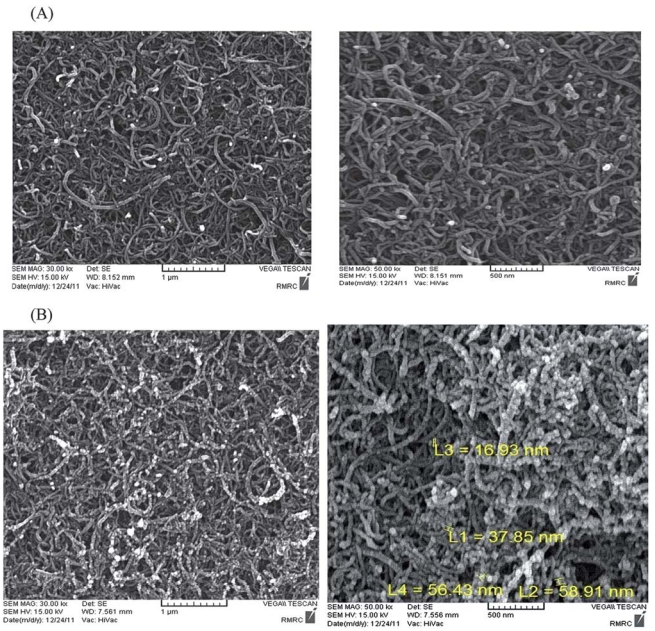

Fig. 1 SEM images with different resolutions of (A) MWCNT and (B) Au–PtNPs/MWCNT modified glassy carbon electrode.

3.2 Structural analysis

The crystalline structure of the Au–PtNPs was characterized by XRD measurement. The XRD pattern for the electrodeposition of Au–PtNPs is shown in Fig. S1.† The wide-angle XRD patterns of the Au–PtNPs/MWCNT showed both Au fcc and Pt fcc peaks, indicating either a mixture or core–shell Au–Pt nanoparticles structure instead of an alloy nanostructure on the electrode surface.[6,31,61]

3.3 Electrochemical characterizations

Fig. 3A shows cyclic voltammetric (CV) profiles obtained in nitrogen-purged 0.1 M PBS of pH 7.0 for different electrodes. For the AuNPs/MWCNT/GC electrode, the reduction peak of the oxide species appeared at about 0.55 V (*vs.* Ag/AgCl). This reduction peak appeared at about 0.09 V (*vs.* Ag/AgCl) for the

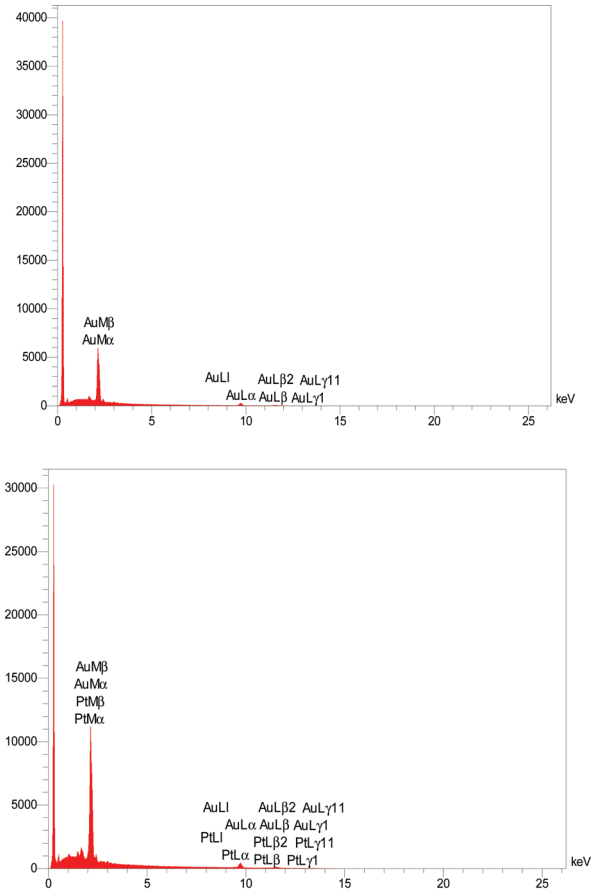

Spectra: CNT/GCE

Element	Line	W%	A%
Carbon	Ka	72.59	95.78
Oxygen	Ka	2.21	2.19
Gold	La	25.19	2.03
	Total:	100.0 %	

Spectra: Au-PtNPs/CNT/GCE

Element	Line	W%	A%
Carbon	Ka	61.56	98.17
Oxygen	Ka	2.24	0.15
Platinum	La	1.88	0.32
Gold	La	34.31	1.21
	Total:	100.0 %	

Fig. 2 The EDS pattern of (A) Au–PtNPs–MWCNT/GCE and (B) MWCNT/GCE.

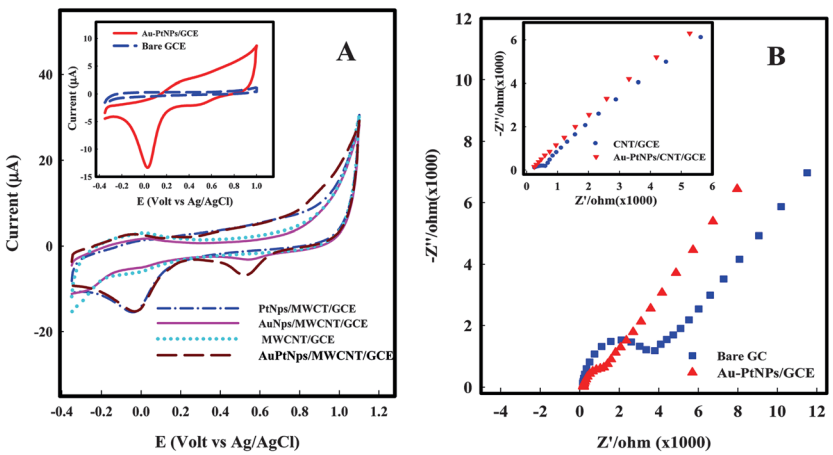

Fig. 3 (A) CVs of Au–PtNPs/MWCNT/GCE (---, brown), MWCNT/GCE (···, cyan), AuNPs/MWCNT/GCE (—, purple) and PtNPs/MWCNT/GCE (-·-, blue) in 0.1 M phosphate buffer solution (pH 7); inset: CVs of Au–PtNPs/GCE (—, red) and bare GCE (---, blue) in the same solution of above. (B) Nyquist diagram ($-Z''$ *vs.* Z') for the EIS measurements in 1 mM $K_3Fe(CN)_6/K_4Fe(CN)_6$ and 0.1 M KCl at $E_{1/2}$ = 0.13 V for a bare GCE (■), Au–PtNPs/GCE (▲); inset: MWCNT/GCE (●), Au–PtNPs/MWCNT/GCE (▼).

PtNPs/MWCNT/GC electrode, due to the reduction of surface platinum oxides. On the other hand, comparison of the cyclic voltammograms for the Au–PtNPs/GC and Au–PtNPs/MWCNT/GC electrode with the bare GC and MWCNT/GC showed two reduction peaks, at about 0.55 V and 0.09 V, which correspond to the reduction of gold and platinum oxide species, respectively.[62,63] Electrochemical impedance spectroscopy (EIS) was employed to investigate the impedance changes and also the interfacial characterization of the electrode surface during the modification processes. Fig. 3B shows the Nyquist plots of K_3Fe

$(CN)_6/K_4Fe(CN)_6$ at the bare GC, Au–PtNPs/GC, MWCNT/GC and the Au–PtNPs/MWCNT/GC. A semicircle with a large diameter is observed at the surface of the bare GC. The diameter of this semicircle is reduced at the Au–PtNPs/GC and Au–PtNPs/MWCNT/GC compared to the bare GC and MWCNT/GC, respectively. These results suggest that the surface of the Au–PtNPs/MWCNT modified electrode exhibits lower electron-transfer resistance and greatly increases the electron-transfer rate. The observed improvements are attributed to a synergistic enhancement rather than merely the combination of bimetallic Au–Pt nanoparticles and carbon nanotube layers. The EIS changes during the modification process also indicated that the Au–PtNPs/MWCNT layer was firmly immobilized on the surface of the GC electrode.

3.4 Electrochemical behavior of various electrodes in CFX oxidation

Fig. 4A illustrates cyclic voltammetric (CV) responses of 10 μM CFX on the surface of the bare GCE, Au–PtNPs/GCE, MWCNT/GCE and Au–PtNPs/MWCNT/GCE. The CFX response has a very weak voltammetric response with an oxidation peak current of 1.3 μA on the surface of the bare GCE. However, in comparison with the bare electrode, a remarkable enhancement in the peak current was observed by a factor of 3.53 ($I_{p,a}$ = 4.6 μA) at the surface of Au–PtNPs/GC. The peak currents of CFX on the surface of MWCNT/GCE and Au–PtNPs/MWCNT/GCE are 17 μA and 26.0 μA that are enhanced respectively by a factor of 13.07 and 20.0 due to the bare GCE. In fact, Au–PtNPs immobilized on the bare GC and MWCNT/GC surfaces with their large surface area increase the adsorptive sites, resulting in a significant increase in the oxidation peak current. On the other hand, in the presence of MWCNT for the modified electrodes, the electrochemical responses toward CFX increase, which is due to the presence of the electroactive oxygenated functional groups and edge sites in the structure of nanotubes, specific electronic structure and high electrical conductivity of MWCNT. We also recorded LSVs of 10 μM CFX oxidation on the surfaces of AuNPs/GC, PtNPs/GC, AuNPs/MWCNT/GCs, and PtNPs/MWCNT/GCs. As shown in Fig. 4B and C, modification of the surface of the bare GCE and MWCNT/GC with AuPt nanoparticles, in comparison to independent contributions from Au or Pt nanoparticles, improved the voltammetric response toward CFX. It should be due to the higher surface area of Au–PtNPs with respect to the Au or Pt NPs alone. Also, in the case of the Au–PtNPs/GC and Au–PtNPs/MWCNT/GC, the stability and reproducibility of the electrode responses to CFX were improved.

3.5 Optimization of the experimental parameters

3.5.1 Influence of pH. The voltammetric investigations were performed in the pH range of 2.0–12.0 using 0.04 M BR buffer solution as supporting electrolyte, containing 10 μM CFX (Fig. 5A). As can be seen in Fig. 5C, the anodic peak potential shows a negative shift by increasing the solution pH with a slope value of 49.8 mV per pH unit (near to the theoretical slope, −59 mV per pH unit). From the results, it can be concluded that equal numbers of electrons and protons are involved in the electro-oxidation of CFX on the surface of the modified electrode.[64] From the results of pH investigations shown in Fig. 5B, BR buffer with pH 2.0 was selected as the supporting electrolyte for obtaining the best sensitivity in all voltammetric determinations.

3.5.2 Effect of potential scan rate. LSVs at different potential sweep rates were used for elucidation of the electrochemical mechanism. Fig. 6A shows LSVs of 10 μM CFX at a modified electrode in a buffered solution of BR (0.04 M, pH 2.0) at different scan rates from 10 to 400 mV s^{-1}. A slope of 0.776 is obtained for the linear variation of the logarithm of the peak current with respect to the logarithm of the sweep rate (Fig. 6B). Observation of such variation can be related to the adsorption of CFX at the modified electrode surface and their diffusion through the porous Pt–AuNPs/MWCNT film.[65] The investigations herein show that increasing the potential scan rate results in a positive shift of the oxidation peak potential with increasing the potential scan rate (Fig. 6C). There is a linear relationship

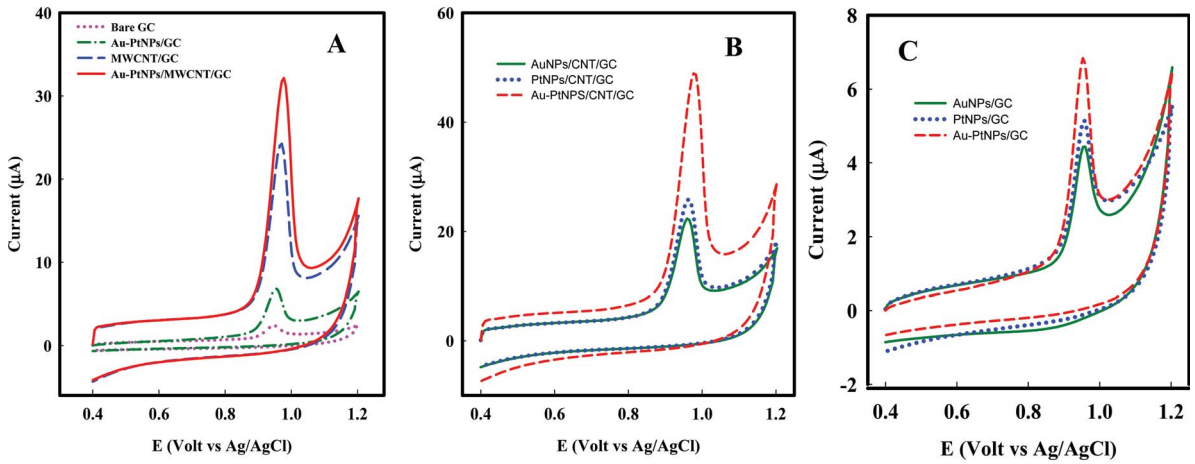

Fig. 4 CVs of 10 μM of CFX on the surface of various electrodes: (A) Au–PtNPs/MWCNT/GCE (—), MWCNT/GCE (---), Au–PtNPs/GCE (-·-) and bare GCE (···); (B) AuNPs/GC (—), PtNPs/GC (···) and Au–PtNPs/GC (---); (C) AuNPs/MWCNT/GC (—), PtNPs/MWCNT/GC (···) and Au–PtNPs/MWCNT/GC (---). Potential sweep rate was 100 mV s^{-1} and supporting electrolyte was 0.04 M BR buffer solution (pH 2.0).

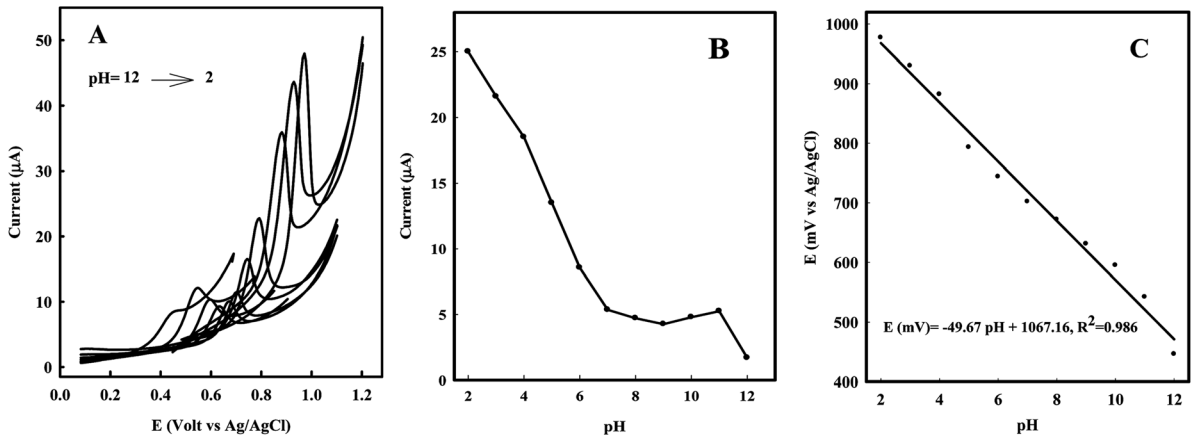

Fig. 5 (A) LSVs of 10 μM CFX at the Au–PtNPs/MWCNT/GCE in various pHs (from 2 to 12) of 0.04 M BR buffer solution. (B) Dependence of oxidation current ($I_{p,a}$) with pH solution. (C) Plot of the oxidation peak potential ($E_{p,a}$) with solution pH; scan rate 100 mV s^{-1}.

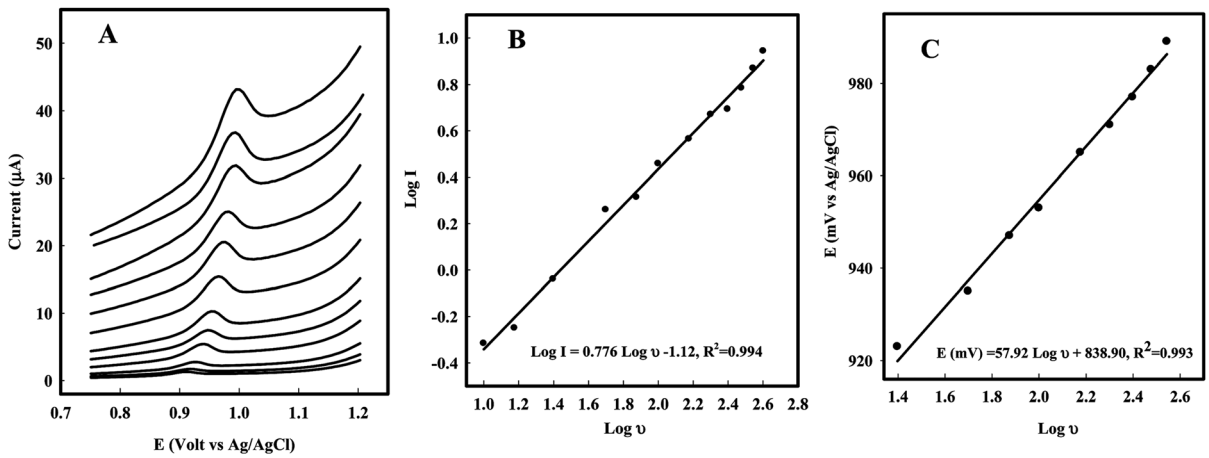

Fig. 6 (A) Effect of potential sweep rate on LSV response of 10 μM CFX (10–400 mV s^{-1}). (B) Plots of log $I_{p,a}$ *vs.* log υ, and (C) variation of peak potentials ($E_{p,a}$) with log υ.

between $E_{p,a}$ and the logarithm of the scan rate, eqn (1), which further reveals the irreversible nature of the electrochemical process:

$$E_{p,a} = 57.92 \log \upsilon + 838.9 \quad (R^2 = 0.993,\ E_{p,a}\text{: mV},\ \upsilon\text{: mV s}^{-1}) \quad (1)$$

For a totally irreversible electrode process (with $\alpha = 0.5$), according to Laviron theory, a value of αn_a as 1.02 can be easily calculated from the slope of *E versus* log υ.[66] So the number of electrons (n) transferred in the electro-oxidation of CFX was calculated to be 2. Integrating the results obtained in pH and scan-rate studies, the electrochemical oxidation of CFX at the Au–PtNPs/MWCNT/GCE should be a two-electron and two-proton process.

3.5.3 Influence of CNT film thickness. In the case of thin film modified electrodes, the current responses toward the analyte species can be affected by the thickness of the modifier film. The film thickness of the porous thin film modified electrode can affect both the kinetics of the electrode processes and the mass transfer mechanism *via* diffusion through the porous film.[67–70] To vary the thickness of the film modifier, different volumes of MWCNT suspension in DMF (1 mg mL^{-1}, 1–4 μL) were deposited on the electrode surface and then the electrochemical response toward CFX was investigated *via* LSV (Fig. 7). The results showed that by increasing the amount of MWCNTs suspension from 0 to 4 μL, a remarkable increase in the oxidation peak current of 10 μM CFX is obtained using the Au–PtNPs/MWCNT/GCE. In our investigations, the optimal CFX response was obtained under conditions employing 3 μL of the MWCNT suspension. Greater suspension volumes of 3 μL resulted in an upper detection limit (about 10 times), inappropriate mechanical properties and decreased the adherence of the MWCNT film onto the GCE surface. Such effects led to a remarkable decrease in the sensitivity and reproducibility of the modified electrode response.

3.5.4 Optimization of accumulation conditions. Cyclic voltammograms of 10 μM CFX at the modified electrode in a BR buffered solution of pH 2 were obtained after a specified accumulation time (data not shown). In the first scan, a well-defined oxidation peak appeared which gradually disappeared in subsequent cycles, resulting from fact that the electrode surface is blocked by the strong adsorption of the CFX or its oxidation

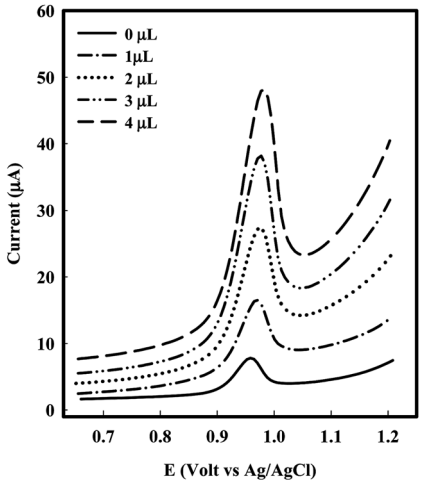

Fig. 7 LSVs of 10 μM CFX at the Au–PtNPs/MWCNT/GCE in various drop sizes of the MWCNT suspension (0–4 μL) cast on the GCE surface.

products. On the other hand, increasing the adsorption time caused an increase in the CFX peak current. These observations indicated that CFX is chemically adsorbed on the electrode surface and then diffuses through the porous Au–PtNPs/MWCNT layer. Therefore, the effects of the accumulation time and corresponding potential parameters were studied in a solution containing 10 μM of CFX. Results showed that longer accumulation times up to 330 s increase the amount of the adsorbed analyte and, therefore, give higher peak currents. With further increase in this time, saturation of the electrode surface was achieved and the peak current remained nearly unchanged. Taking account of sensitivity and also response repeatability, the accumulation time was set at 330 s in the following experiments (Fig. 8). It was found that accumulation potential has no influence on the oxidation peak current. The results showed that, in comparison to the open circuit conditions, the oxidation peak current remained almost constant when the accumulation potential was applied. Therefore, accumulation of CFX was performed under open circuit conditions.

3.6 Analytical characteristics and methods validation

The practical applicability of the proposed method was evaluated by investigating the analytical performance characteristics such as linear range, detection limit, repeatability and reproducibility under the optimized conditions. The results of the voltammetric studies for various concentrations of CFX on the surface of the Au–PtNPs/MWCNT/GCE are shown in Fig. 9A. Using the plot of peak currents *versus* the concentration of CFX, two linear ranges of 0.004–4.0 μM and 4.0–10.0 μM in 0.04 M BR solution (pH 2) were obtained (Fig. 9B). Linear regression equations for these two regions were:

$$I\,(\mu A) = 4.76C_{CFX}\,(\mu M) + 0.26 \quad (R^2 = 0.994) \qquad (2)$$

$$I\,(\mu A) = 1.3C_{CFX}\,(\mu M) + 13.6 \quad (R^2 = 0.993) \qquad (3)$$

A detection limit of 1 nM (based on $S/N = 3$) was obtained for CFX using the first range of the calibration plot. Table 1 compares the response characteristics of the Au–PtNPs/MWCNT/GCE with those of other modified electrodes reported in the literature for the determination of CFX. As can be seen, in comparison with the previous works, the present method exhibits the lowest limit of detection, the highest sensitivity and widest linear dynamic ranges (more than 3 orders of magnitude) for the electrochemical determination of CFX. To study the reproducibility of the electrode preparation procedure, five electrodes modified by a same fabrication procedure were prepared and used for the determination of a 10 μM solution of CFX. The RSD for the electrodes' peak currents (average of three determinations on each electrode) was calculated to be 3.96%. To determine the precision of the method, electrochemical experiments were repeated 5 times with the same Au–PtNPs/MWCNT/GCE in solution containing 10 μM of CFX. The RSD was calculated to be 2.16%. In this work, any adsorbed CFX or its oxidation product was counteracted by applying ten CVs in supporting electrolyte (BR) between measurements, thereby obviating the fouling problems and renewing the electrode surface. Thus, the results herein indicate that the modified

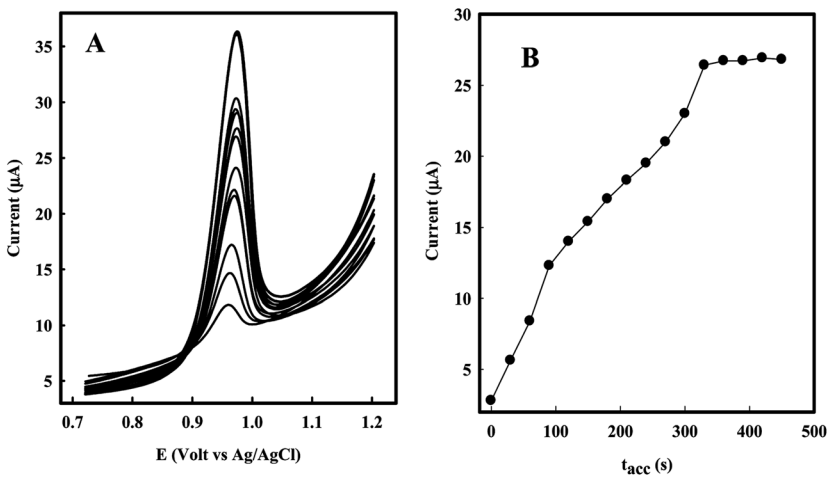

Fig. 8 (A) Effect of accumulation time, t_{acc}(s), on LSVs of 10 μM of CFX on the surface of the Au–PtNPs/MWCNT/GCE in 0.04 M BR buffer solution (pH 2.0). (B) Plot of current *versus* accumulation time for different concentrations of CFX.

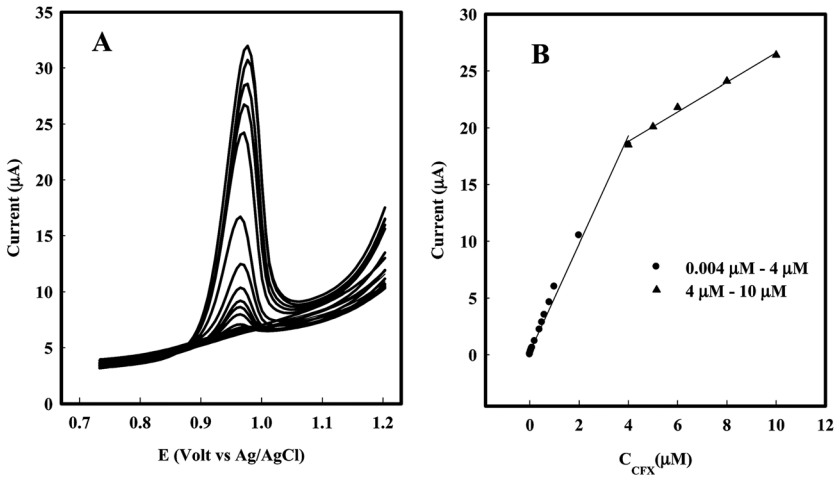

Fig. 9 (A) LSVs for various concentrations of CFX in the range of 0.004–10 μM supporting electrolyte was 0.04 M BR buffer solution (pH 2.0). (B) Corresponding linear calibration curve of peak current *vs.* CFX concentration.

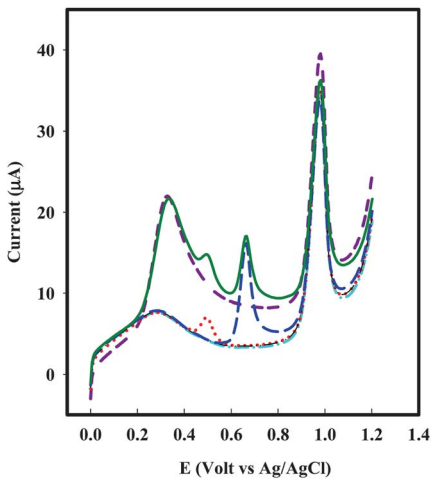

Fig. 10 LSVs of Au–PtNPs/MWCNT/GCE for the determination of 10 μM cefotaxime (-·-, cyan) and 10 μM cefotaxime in the presence of 1 mM AA (---, purple), 0.1 mM UA (---, blue), 10 μM DP (···, red), 1 mM Glu (—··—, black) and the mixture of AA, UA, DP and Glu interferences (—, green) in 0.04 M BR buffer solution (pH 2.0). Scan rate: 100 mV s^{-1}.

electrode has an excellent repeatability in both preparation and determination steps. In the present work, the interference effects of 1 mM ascorbic acid (AA), 0.1 mM uric acid (UA), 10 μM dopamine (DP) and 1 mM glucose (Glu) were tested on the voltammetric response of 10 μM CFX (Fig. 10). No change in the response current of CFX was observed in the presence of these compounds or mixtures of them. In the mixture of all these compounds by using the modified electrode, four well-defined waves with a very good resolution are obtained. Among these interferences, glucose has no response but AA, UA, and DP showed an oxidation process in the selected potential range. Therefore, in this study it was proved that this method can be successfully applied for the simultaneous determination of cefotaxime in the presence of the other interference compounds in the clinical preparations.

3.7 Applicability of sensor to real matrixes

3.7.1 Determination of CFX in ampoule sample. Because components of the matrix of the drug may interfere with the accurate determination of the analyte, potential effects from matrix components must be investigated. So, the reliability of the modified electrode was assessed for determination of CFX ampoules using a standard addition recovery method. A CFX ampoule was diluted to 500 mL by 0.04 M BR buffer solution (pH 2) to get an approximate concentration of 10 μM. A 2.5 mL portion of the resulting solution was added to the standard CFX solutions (in the range of 4–10 μM) and the samples were diluted to 25.0 mL. The voltammetric response and corresponding calibration plot of peak currents *versus* concentration are shown

Table 1 Comparison of different modified electrodes for determination of CFX

Electrode	Method	Linear range/μM)	Sensitivity/μA μM^{-1}	LOD/nM	Ref.
Zn(II)complex/graphite paste electrode	DPV[a]	0.001–0.05, 0.1–50	N[f]	N	58
Activated GCE	HFSWV[b]	20–100, 200–600	0.005, 0.017	N	57
Dropping mercury electrode (DME)	AdSDP[c]	0.15–1.1	0.4	N	53
Hanging mercury dropping electrode (HMDE)	SWAdSV[d]	0.007–0.10, 0.12–1.2	3.03, 5.27	1.7	55
Au–PtNPs/MWCNT/GC	LSV[e]	0.004–4, 4–10	4.76, 1.3	1	This work

[a] Differential potential voltammetry. [b] High-frequency square wave voltammetry. [c] Adsorptive stripping differential pulse voltammetry. [d] Square wave adsorptive stripping voltammetry. [e] Linear sweep voltammetry. [f] Not reported.

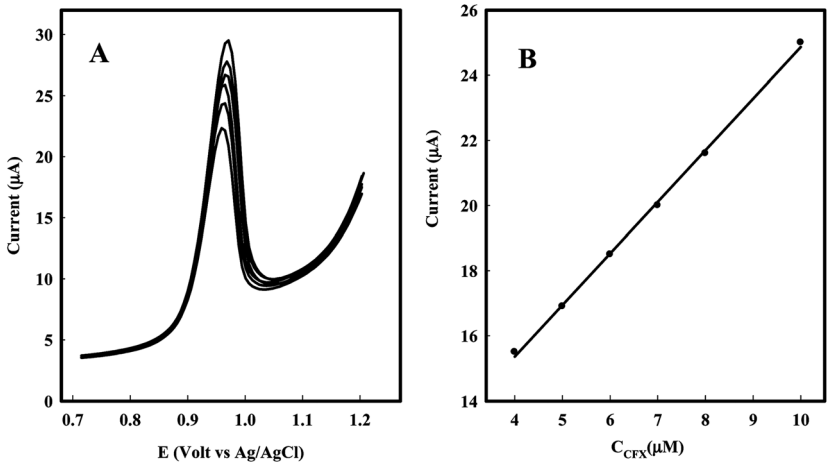

Fig. 11 (A) LSVs for the addition of the different amounts of CFX (4, 5, 6, 7, 8 and 10 μM) in the real sample solution of CFX diluted with 0.04 M BR buffer solution (pH 2.0) and (B) the plot of peak current *vs.* added concentration of CFX.

Table 2 Recovery results of CFX analysis spiked in plasma samples[a]

No	Spiked/μM	Found/μM	Recovery (%)	RSD (%)
1	0.01	0.009	95.06	1.29
2	0.1	0.104	104.36	2.85
3	0.6	0.660	110.00	3.46
4	2.0	1.931	96.56	5.87

[a] Mean ± standard deviation ($n = 3$) (rounded).

in Fig. 11A and B. The equation for resulting standard addition calibration curve was:

$$I\,(\mu A) = 1.26C_{CFX}\,(\mu M) + 10.6 \quad (R^2 = 0.997) \qquad (4)$$

By comparing two slopes of the standard and spiked drug samples, it is concluded that no interferences in the drug matrix were found for the electrochemical analysis of CFX. An amount of 483.87 mg with a good accuracy of 96.77% and an RSD of 3.86% ($n = 3$) was found for the analysis of drug samples. Moreover, for accuracy studies, recoveries were evaluated in the lower, middle and higher level concentrations of the spiked CFX to the pharmaceutical solutions. The recoveries were in the range from 106.87 to 95.92%.

3.7.2 Determination of CFX in human plasma. For preparation of serum samples, 2% (v/v) of methanol was added to the human serum sample and thoroughly mixed. Then, the plasma samples were diluted 10 times with BR buffer solution (pH 2). Recovery evaluation of CFX was carried out by spiking of its standard solutions in the range of 0.01–4 μM into the diluted plasma samples. The modified electrode was applied for analysis of these samples. The results showed an average recovery of 96.28% for CFX added to the human serum samples (Table 2).

4 Conclusion

In conclusion, we have successfully prepared the Au–PtNPs/MWCNT/GCE by consecutive electrochemical deposition of AuNPs and PtNPs onto an MWCNT film pre-casted on the surface of a glassy carbon electrode at room temperature for a short time. This modified electrode is used as an enhanced material for the sensitive voltammetric determination of cefotaxime. The highly effective microscopic area of the Au–PtNPs/MWCNT modifier together with effective accumulation of CFX at the electrode surface resulted in a considerable increase in the obtained peak currents. The modified electrode also has other remarkable electrochemical advantages such as high reproducibility, excellent repeatability, antifouling behavior, wide linear dynamic range (more than 3 orders of magnitude) and nanomolar detection limit that provide the successful application of this sensor for the determinations of CFX in pharmaceutical and clinical preparations.

Acknowledgements

The authors gratefully acknowledge the support of this work by the Research Council and the Center of Excellence for Nanostructures of the Sharif University of Technology, Tehran, Iran. We are thankful to Exir Daru pharmaceutical company (Tehran–Iran) for getting us kindly the cefotaxime drug.

References

1 F. W. Campbell and R. G. Compton, *Anal. Bioanal. Chem.*, 2010, **396**, 241–259.
2 F. W. Campbell, S. R. Belding and R. G. Compton, *ChemPhysChem*, 2010, **11**, 2820–2824.
3 Y. G. Zhou, F. W. Campbell, S. R. Belding and R. G. Compton, *Chem. Phys. Lett.*, 2010, **497**, 200–204.
4 K. E. Toghill and R. G. Compton, *Electroanalysis*, 2010, **22**, 1947–1956.
5 T. J. Davies, C. E. Banks and R. G. Compton, *J. Solid State Electrochem.*, 2005, **9**, 797–808.
6 F. Xiao, F. Zhao, Y. Zhang, G. Gaiping and B. Zeng, *J. Phys. Chem. C*, 2009, **113**, 849–855.
7 (*a*) Y. Shin, I. Bae, B. W. Arey and G. J. Exarhos, *J. Phys. Chem. C*, 2008, **112**, 4844–4848; (*b*) J. H. Liu, A. Q. Wang, Y. S. Chi, H. P. Lin and C. Y. Mou, *J. Phys. Chem. B*, 2005, **109**, 40–43.
8 W. Q. Tian, M. Ge, F. Gu, T. Yamada and Y. Aoki, *J. Phys. Chem. A*, 2006, **110**, 6285–6293.
9 Y. Du, Y. Qiao, C. Zou, J. Dai and P. Yang, *Colloid Polym. Sci.*, 2007, **285**, 553–556.

10 B. E. Roustom, G. Siné, G. Fóti and Ch. Comninellis, *J. Appl. Electrochem.*, 2007, **37**, 1227–1236.
11 Y. Song, Y. Ma, Y. Wang, J. Di and Y. Tu, *Electrochim. Acta*, 2010, **55**, 4909–4914.
12 D. Vairavapandian, P. Vichchulada and M. D. Lay, *Anal. Chim. Acta*, 2008, **626**, 119–129.
13 P. Yanez-Sedeno, J. Riu, J. M. Pingarron and F. X. Rius, *TrAC, Trends Anal. Chem.*, 2010, **29**, 939–953.
14 C. B. Jacobs, M. J. Peairs and B. J. Venton, *Anal. Chim. Acta*, 2010, **662**, 105–127.
15 N. Y. Hsu, C. C. Chien and K. T. Jeng, *Appl. Catal., B*, 2008, **84**, 196–203.
16 S. Shahrokhian, M. Ghalkhani, M. Adeli and M. K. Amini, *Biosens. Bioelectron.*, 2009, **24**, 3235–3241.
17 M. Ghalkhani, S. Shahrokhian and F. Ghorbani-Bidkorbeh, *Talanta*, 2009, **80**, 31–38.
18 S. Shahrokhian and S. Rastgar, *Electrochim. Acta*, 2011, **58**, 125–133.
19 S. Arai, M. Endo and N. Kaneko, *Carbon*, 2004, **42**, 641–644.
20 B. Rohland, M. Pietrzak, S. Moeller, M.-C. Bunescu, M. Wienecke, T. Barfels and M. C. Bunescu, *Fullerenes, Nanotubes, Carbon Nanostruct.*, 2005, **13**, 511–522.
21 W.-X. Chen, J. Y. Lee and Z. Liu, *Mater. Lett.*, 2004, **58**, 3166–3169.
22 M. Carmo, V. A. Paganin, J. M. Rosolen and E. R. Gonzalez, *J. Power Sources*, 2005, **142**, 169–176.
23 L. Han, W. Wu, F. L. Kirk, J. Luo, M. M. Maye, N. N. Kariuki, Y. Lin, C. Wang and C.-J. Zhong, *Langmuir*, 2004, **20**, 6019–6025.
24 G. G. Wildgoose, C. E. Banks and R. G. Compton, *Small*, 2006, **2**, 182–193.
25 T. M. Day, P. R. Unwin and J. V. Macpherson, *Nano Lett.*, 2007, **7**, 51–57.
26 C. B. Hwang, Y. S. Fu and S. J. Yu, *J. Catal.*, 2000, **195**, 336–341.
27 L. Yang, J. Chen, X. Zhong, K. Cui, Y. Xu and Y. Kuang, *Colloids Surf., A*, 2007, **295**, 21–26.
28 F. Terzi, C. Zanardi, S. Daolio, M. Fabrizio and R. Seeber, *Electrochim. Acta*, 2011, **56**, 3673–3678.
29 J. Wang, G. Yin, H. Liu, R. Li, R. L. Fleming and X. Sun, *J. Power Sources*, 2009, **194**, 668–673.
30 J. Luo, P. N. Njoki, Y. Lin, D. Mott, L. Wang and C. J. Zhong, *Langmuir*, 2006, **22**, 2892–2898.
31 F. Xiao, Z. Mo, F. Zhao and B. Zeng, *Electrochem. Commun.*, 2008, **10**, 1740–1743.
32 J. Zhai, M. Huang and S. Dong, *Electroanalysis*, 2007, **19**, 506–509.
33 Y. C. Bai, W. D. Zhang, C. H. Chen and J. Q. Zhang, *J. Alloys Compd.*, 2011, **509**, 1029–1033.
34 Y. C. Bai and W. D. Zhang, *Electroanalysis*, 2010, **22**, 237–243.
35 F. Xiao, F. Zhao, D. Mei, Z. Mo and B. Zeng, *Biosens. Bioelectron.*, 2009, **24**, 3481–3486.
36 Y. Zhang, G. Guo, F. Zhao, Z. Mo, F. Xiao and B. Zeng, *Electroanalysis*, 2010, **22**, 223–228.
37 X. Kang, Z. Mai, X. Zou, P. Cai and J. Mo, *Anal. Biochem.*, 2007, **369**, 71–79.
38 A. Safavi and F. Farjami, *Biosens. Bioelectron.*, 2011, **26**, 2547–2552.
39 A. Gringauz, *Introduction to Medicinal Chemistry*, Wiley-VCH, New York, 1997, p. 216.
40 L. P. Morrelli, *Analytical Profile of Drug Substances*, Academic Press, 1975, vol. 4, p. 21.
41 S. M. Berge, N. L. Henderson and M. J. Frank, *J. Pharm. Sci.*, 1983, **72**, 59–63.
42 K. A. Connors, *Chemical Stability of Pharmaceuticals*, Wiley-Interscience Publication, John Wiley & Sons, New York, 1986, p. 302.
43 D. Chen, H. Wang, Z. Zhang, L. Ci and X. Zhang, *Spectrochim. Acta, Part A*, 2011, **78**, 553–557.
44 Z. Wang, Z. Song and D. Chen, *Talanta*, 2010, **83**, 312–319.
45 M. A. Omar, O. H. Abdelmageed and T. Z. Attia, *Talanta*, 2009, **77**, 1394–1404.
46 A. S. Amin and G. H. Ragab, *Spectrochim. Acta, Part A*, 2004, **60**, 2831–2835.
47 H. Salem and H. Askal, *J. Pharm. Biomed. Anal.*, 2002, **29**, 347–354.
48 T. Ohmori, A. Suzuki, T. Niwa, H. Ushikoshi, K. Shirai, S. Yoshida, S. Ogura and Y. Ito, *J. Chromatogr., B: Anal. Technol. Biomed. Life Sci.*, 2011, **879**, 1038–1042.
49 Q. Liu, L. Xu, Y. Ke, Y. Jin, F. Zhang and X. Liang, *J. Pharm. Biomed. Anal.*, 2011, **54**, 623–628.
50 M. T. Rosseel and K. H. Vandewoude, *J. Chromatogr., B: Anal. Technol. Biomed. Life Sci.*, 2004, **811**, 159–163.
51 V. F. Samanidou, A. S. Ioannou and I. N. Papadoyannis, *J. Chromatogr., B: Anal. Technol. Biomed. Life Sci.*, 2004, **809**, 175–182.
52 S. S. N. Ling, K. H. Yuen and S. A. Barker, *J. Chromatogr., B: Anal. Technol. Biomed. Life Sci.*, 2003, **783**, 297–301.
53 M. M. Aleksic, V. Kapetanovic, J. Atanackovic, B. Jocic and M. Zecevic, *Talanta*, 2008, **77**, 131–137.
54 N. A. El-Maali, A. H. Osman, A. A. M. Aly and G. A. A. Al-Hazmi, *Bioelectrochemistry*, 2005, **65**, 95–104.
55 M. M. Aleksic and V. Kapetanovic, *J. Electroanal. Chem.*, 2006, **593**, 258–266.
56 E. Munoz, J. L. Avila, J. P. Doctor and L. Camacho, *Electroanalysis*, 1993, **5**, 325–331.
57 N. Yılmaz and I. Biryol, *J. Pharm. Biomed. Anal.*, 1998, **17**, 1335–1344.
58 P. Nigam, S. Mohan, S. Kundu and R. Prakash, *Talanta*, 2009, **77**, 1426–1431.
59 H. Fabre, M. D. Blanchin and U. Tjaden, *Analyst*, 1986, **111**, 1281–1284.
60 N. Abo El-Maali, M. A. Ghandour and J. M. Kauffmann, *Bioelectrochem. Bioenerg.*, 1995, **38**, 91–97.
61 H. A. Esfahani, L. Wang, Y. Nemoto and Y. Yamauchi, *Chem. Mater.*, 2010, **22**, 6310–6318.
62 Y. Ma, H. Zhang, H. Zhong, T. Xu, H. Jin and X. Geng, *Catal. Commun.*, 2010, **11**, 434–437.
63 Y. Song, Y. Ma, Y. Wang, J. Di and Y. Tu, *Electrochim. Acta*, 2010, **55**, 4909–4914.
64 E. Laviron, *J. Electroanal. Chem.*, 1974, **52**, 355–365.
65 R. S. Nicholson and I. Shain, *Anal. Chem.*, 1964, **36**, 706–723.
66 E. Laviron, *J. Electroanal. Chem.*, 1979, **101**, 19–28.
67 I. Streeter, G. G. Wildgoose, L. Shao and R. G. Compton, *Sens. Actuators, B*, 2008, **133**, 462–466.
68 L. Xiao, L. Wi, G. G. Wildgoose and R. G. Compton, *Sens. Actuators, B*, 2009, **138**, 524–531.
69 M. C. Henstridge, *Sens. Actuators, B*, 2010, **145**, 417–427.
70 G. P. Keeley and M. E. G. Lyons, *Int. J. Electrochem. Sci.*, 2009, **4**, 794–809.